





## Interplay of boundary states of graphene nanoribbons with a Kondo impurity

Sujoy Karan <sup>1,2</sup>, Tobias Frank,<sup>3,\*</sup> Tobias Preis <sup>1</sup>, Jonathan Eroms <sup>1</sup>, Jaroslav Fabian <sup>3</sup>, Ferdinand Evers <sup>3</sup>,  
and Jascha Repp <sup>1,†</sup>

<sup>1</sup>*Institute of Experimental and Applied Physics, University of Regensburg, 93040 Regensburg, Germany*

<sup>2</sup>*Max Planck Institute for Solid State Research, Heisenbergstraße 1, 70569 Stuttgart, Germany*

<sup>3</sup>*Institute of Theoretical Physics, University of Regensburg, 93040 Regensburg, Germany*

 (Received 28 September 2021; revised 19 April 2022; accepted 25 April 2022; published 6 May 2022)

We investigate the interplay of two highly localized, nearly degenerate electronic states, namely, a zero-energy edge mode in a graphene nanoribbon on the one hand and an Abrikosov-Suhl resonance located at a Kondo impurity on the other. On-surface synthesis of the ribbon structures in combination with intercalation of single-atom Kondo impurities by atomic manipulation in a scanning tunneling microscope junction offer full control of the atomic geometry of the system. Density functional theory provides the microscopic description to scrutinize the electronic features observed in experiment. We find the interaction of the two localized states and the resulting signatures of Kondo physics to be very sensitive to the placing of the atom, suggesting its use as a laboratory to study the interplay of the Kondo effect with other zero-bias anomalies as well as to tailor these states by controlling the atomic-scale coupling.

DOI: [10.1103/PhysRevB.105.205410](https://doi.org/10.1103/PhysRevB.105.205410)

### I. INTRODUCTION

Graphene nanoribbons (GNRs), the quasi-one-dimensional graphene, have been proposed as building blocks for future nanoelectronic devices owing to their versatility. While offering a tunable band gap [1–3], they can be synthesized with atomic perfection in a large variety of widths [4–9] and shapes [9–13] and even regular chemical doping [14–17] can be directly implemented in the synthesis process. Moreover, the honeycomb structure of the underlying graphene lattice allows one to further tailor the electronic properties by the ribbon's atomic structure [18–20]. For example, a (local) zigzag edge termination introduces singly occupied in-gap states [21]. These singly occupied states arising from such edge terminations can give rise to magnetic moments that are localized at the edges [19,22–26].

Such edge states or, more generally speaking, boundary states, manifest as strong resonances in the local density of states (LDOS), close to the Fermi energy  $E_F$ . Quite generally, the vicinity of strong features in  $\text{LDOS}(E)$  near  $E_F$  makes boundaries an interesting laboratory for Kondo physics. For example, for Kondo impurities embedded in Dirac metals, the suppression of the LDOS near the charge neutrality point results in a systematic decrease of Kondo temperatures  $T_K$  (Ref. [27]) or even stronger modifications including a breakdown of Kondo screening (pseudogap Kondo model [28]). In view of this, GNRs adsorbed on a metal surface represent an attractive test bed for Kondo phenomena [29] because they provide an embedding that can be tuned. At the same time, these systems allow for an atomic control of the geometry and thus of the coupling between a Kondo impurity and localized boundary states [30].

Specifically, in our experiments we consider a Co atom as Kondo impurity. It is situated between the substrate, i.e., Au(111), and a seven-unit-cell-wide armchair GNR (7-aGNR) synthesized on this surface [9]. Co shows a strong Kondo feature on Au(111) [31]. The intercalation of Co atoms below or away from the boundary of aGNR is achieved with atomic precision. Since the LDOS of the aGNR, and therefore the hybridization of the Co atom with its embedding, is very sensitive to the placing of the atom, so will be the signatures of Kondo physics. This general expectation is nicely met by the experiments we report here.

To highlight our observations from another angle, we put them into context with molecular electronics. From this perspective, our experimental system is an organometallic complex contacted to source (substrate) and drain (tip). A plethora of correlation phenomena can occur in such hybrid systems including flavors of Kondo physics that have not occurred otherwise (see Ref. [32] for a recent overview). An aspect of our work with respect to these developments is the superior control and flexibility of the atomic system structure.

7-aGNRs host three zigzag cusps, predicted to be enough to give rise to singly occupied in-gap states, at their short edges such that two midgap states, each localized at one of their ends, are expected. Indeed, the occurrence of such midgap states, henceforth referred to as end states, has been reported for 7-aGNRs on Au(111) [33,34], which decay within a short distance of  $\sim 1.5$  nm from the zigzag termini [35]. These end states shift slightly above the Fermi level due to hole doping of the 7-aGNR on Au(111) [36]. Apart from a signal in differential conductance spectra, the end state exhibits a fingerlike structure in scanning tunneling microscopy (STM) images at the zigzag termini [37]. While within one zigzag edge magnetic moments typically favor ferromagnetic ordering [1,38], antiferromagnetic ordering is favorable between opposing edges [38,39], rendering  $A$ - $B$ -

\*tobias.frank@physik.uni-regensburg.de

†jascha.repp@physik.uni-regensburg.de

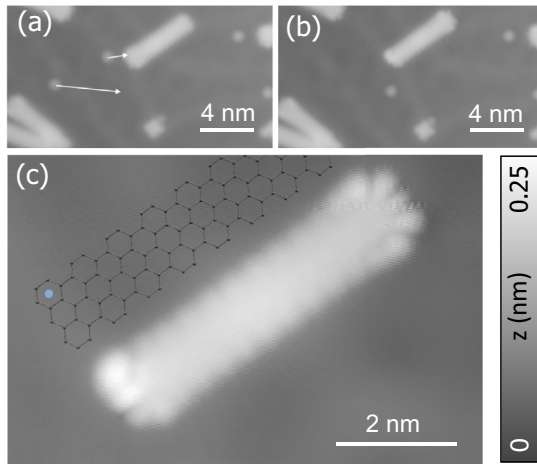


FIG. 1. Assembly of Co-GNR complexes. (a), (b) Manipulation of Co atoms across the surface and underneath the GNR.  $V = 100$  mV,  $I = 11$  pA. (c) High-resolution STM image of the Co-GNR complex. The model shows magnified sketch of the Co intercalation position. Gray spheres depict C atoms and blue Co, respectively.  $V = 2$  mV,  $I = 48$  pA.

sublattice-balanced GNR spin neutral in accordance to Lieb's theorem [40].

In the sections below, we describe how the intercalation of individual Co atoms (Sec. II A) under a GNR influences its intrinsic boundary states (Sec. II B) to result in a site-specific electronic transport as the Co atom is moved from the corner of a ribbon (Sec. II C) along the armchair edge to the bulk (Sec. II D). Furthermore, GNR complexes with Au atoms intercalated below a corner site (Sec. II E) add attributing and understanding Co unpaired electron being involved in the process.

## II. RESULTS

### A. Atomic structure: Intercalation of adatoms

*Experiment.* To study the local interaction of the GNR with individual Co impurity adatoms, we take advantage of atom manipulation [41,42] and bring individual Co adatoms in direct contact with the 7-aGNRs in a controlled manner [see Figs. 1(a) and 1(b)], resulting in Co-GNR complexes with Co being intercalated beneath one of the benzene rings of the GNR. We note that after deposition we observed Co atoms residing also on top of GNRs, with a distinctly different appearance in STM images [43]. We therefore safely rule out the possibilities of Co being manipulated on to the top of GNR.

Inspection of images before and after the manipulation reveals that the GNR moves laterally toward the adatom during the intercalation process, in this particular example by 0.9 nm. Such snap-in-place motion occurred frequently during the assembly of Co-GNR complexes and suggests an attractive interaction between the adatom and the GNR with a preferred intercalation position.

*Theory.* To highlight the details of the atomic structure, we display in Fig. 2 the geometry as obtained from the density functional theory (DFT). The carbon atoms away from the

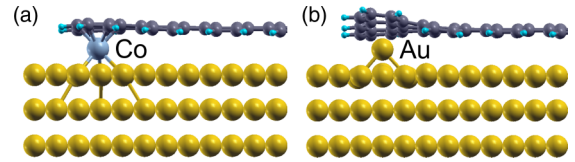


FIG. 2. Au vs Co at GNR corner. DFT calculated side views of (a) a Co(1)-GNR complex and (b) a Au(1)-GNR complex revealing larger GNR distortion.

intercalation site exhibit an average distance of about 3.1 Å, in broad agreement with simulations of bulk graphene on gold with a van der Waals gap of 3.3 Å [44].<sup>1</sup> Carbon atoms at the intercalation position (the hexagonal carbon ring) are pushed away residing about 3.3 Å above the substrate in the case of Co [Fig. 2(a)]. The excess of 0.2 Å is in reasonable agreement with the experimental value of 0.3 Å (see further below). For an intercalating Au atom the effect is seen to be even stronger [Fig. 2(b)], presumably reflecting its larger (calculated) size and a different binding chemistry with substrate and GNR. We obtain an excess of 1.0 Å. Calculations are in qualitative agreement with experiment (cf. Fig. 9).

### B. End-state appearance

*Experiment.* During the process of manipulation from Fig. 1(a) to 1(b), the fingerlike structure characteristic to the end state appeared at the pristine GNR end (see top-right end). Similar subtle changes in the electronic structure at the end of the GNR opposite to the intercalation were observed occasionally during the manipulation. A modification of the end state in GNRs can be induced by hydrogen elimination [34]. Here, however, the pristine GNR end was exposed to very moderate bias conditions for imaging ( $V = 100$  mV,  $I = 11$  pA).

We therefore attribute the reappearance of the fingerlike structure of the end state to the change in adsorption configuration resulting from the snap-in-place motion. We speculate that some adsorption configurations feature a stronger interaction between certain gold atoms in the herringbone-reconstructed surface which may lead to a suppression of the end state, which will thus recover if the GNR is displaced on the surface. This explanation is in line with the observation made in Ref. [45] that certain nanographene-like molecules are pinned to the elbows of the Au(111) herringbone ridges. These observations underscore that the role of the substrate must be considered when interpreting subtle changes in the electronic structure of adsorbed GNRs.

*Theory.* Since the GNR in the absence of intercalation is only physisorbed on the substrate, its weakly perturbed electronic structure is conveniently described and is discussed on the tight-binding level. The model considers the atomic geometry displayed in Fig. 3(a) with nearest-neighbor hopping

<sup>1</sup>The difference between 3.1 and 3.3 Å is due to the different exchange-correlation functional and van der Waals corrections employed, which is LDA without corrections in Ref. [75] and PBE with empirical van der Waals corrections in this work.

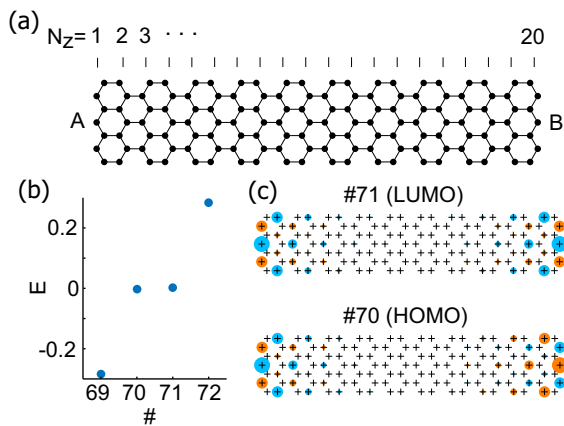


FIG. 3. Tight-binding setup. (a) Model used for the tight-binding calculations containing 140 carbon atoms. Left GNR zigzag edge consists of  $A$  atoms only, right edge of  $B$  atoms. (b) Energy of the states closest to  $E_F$  in units of the nearest-neighbor hopping integral  $t$ . (c) Real-space distribution of the wave functions of HOMO and LUMO of the GNR, where disk size indicates the modulus of the wave function and color encodes the sign.

$t \approx 3$  eV [46]; as an energy reference we consider the band center.

An infinitely long GNR with a width displayed in Fig. 3(a) is expected to be a band insulator with a gap of the order of 1 eV [47]. Due to the bipartite nature of the honeycomb lattice, the corresponding band structure is symmetric around zero energy (Coulson-Rushbrooke pairs) [32,48]. The appearance of the end state is understood as follows: a pair of end states is created by cutting the infinite ribbon into two semi-infinite segments. In the process, three bonds are cut leading to three radicals per segment. Due to the insulating nature of the GNR's bulk, i.e., those regions of the ribbon far away from the short edges, these radicals are confined to the ends where they form an edge band. Owing to the spectral symmetry, i.e., Coulson-Rushbrooke pairing, an edge with an odd number of radicals will exhibit one zero-energy state, the end state. We mention that the consequences of (broken) bipartiteness and a sublattice mismatch in GNRs have received a significant recent interest [49–51].

In our tight-binding calculations we consider a GNR of finite length [Fig. 3(a)]. It features a left and right end state that experience an exponentially small coupling via tunneling through the GNR's bulk. Consequently, the spectrum exhibits two near-zero energy modes, HOMO and LUMO, that are even and odd combinations of end states [see Fig. 3(b)]. In the charge-neutral situation, the HOMO is doubly occupied, forming a nonmagnetic ground state  $S = 0$  [Fig. 3(c)]. However, due to the Coulomb repulsion between the two electrons, this state is not stable; instead, HOMO and LUMO will re-hybridize, so that eventually each end state carries a single electron with well-defined spin.

### C. Co at corner site

*Experiment.* A high-resolution STM image of the Co-GNR complex [see Fig. 1(c)] exhibits a bright, roundish protrusion at the GNR corner, where Co was intercalated. A more de-

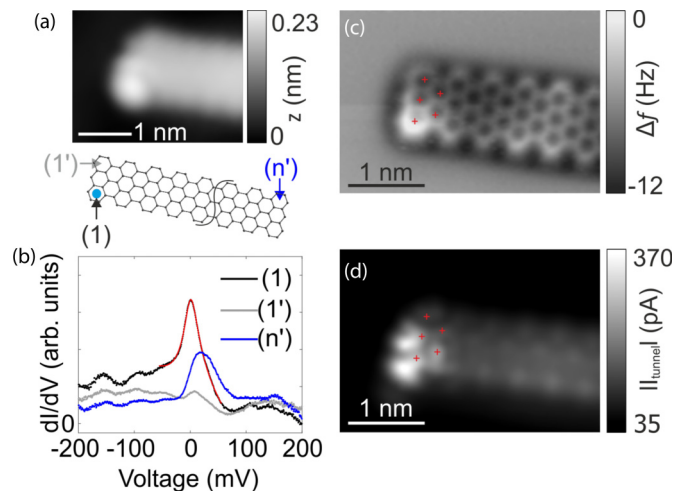


FIG. 4. Co at corner site. (a) STM image of a Co(1)-GNR complex ( $V = 5$  mV,  $I = 30$  pA, mild Gaussian smoothing applied) along with a sketch of the configuration. (b)  $dI/dV$  spectra taken at positions indicated in the sketch in (a). Red curve indicates a fit of an asymmetric Frotta line. (c) Constant height AFM image and (d) current map of the complex shown in (a). Red crosses in (c) and (d) mark the same positions.

tailed view of such a Co-GNR end is shown in Fig. 4(a). The fingerlike structure typical of the end state is absent at the Co-GNR end. Figure 4(c) shows a constant-height atomic force microscopy (AFM) image recorded with a CO-terminated tip. The carbon ring at the corner of the GNR is imaged more repulsive as compared to the other rings, but otherwise exhibits the intact honeycomb structure of graphene. This supports the assumption that the Co atoms are indeed intercalated in-between the GNR and the gold support. Further, it suggests that the intercalation position is at the center of a corner  $C_6$  ring. In fact, this position is the energetically most favorable adsorption position for most adatoms on graphene [52,53]. Moreover, calculations for various transition metal atoms adsorbed on aGNRs of different widths indicated that binding to the outermost carbon ring, i. e., the one at the armchair edge, is energetically most stable [54]. The more repulsive interaction of the corner ring in Fig. 4(c) suggests that it is lifted away from the surface because of the intercalation of the Co adatom. To quantify this further, we applied a technique proposed in Ref. [55] and determined the minimum in  $\Delta f$  as a function of tip height  $z$  for different lateral positions. The tip height, at which  $\Delta f(z)$  is minimized, increases by  $\sim 0.3$  Å upon Co intercalation, suggesting that the corner ring is pushed away from the surface by this distance.

For an electronic characterization, differential conductance ( $dI/dV$ ) spectra were acquired at the positions indicated by color-coded arrows in Fig. 4(b). The spectrum taken at the corner site far away from the Co (labeled  $n'$ ), namely, the pristine GNR end, exhibits the signature of the well-known end state featuring a peak at  $21 \pm 3$  mV with a full width at half-maximum (FWHM) of  $42 \pm 15$  mV [see Fig. 4(b) (blue curve)]. We note that, for different ribbons, these end states are found to appear at different energy positions (mostly within the range of 10 to 40 meV) and exhibit different FWHM values scattered approximately around  $40 \pm 25$  mV. In contrast,

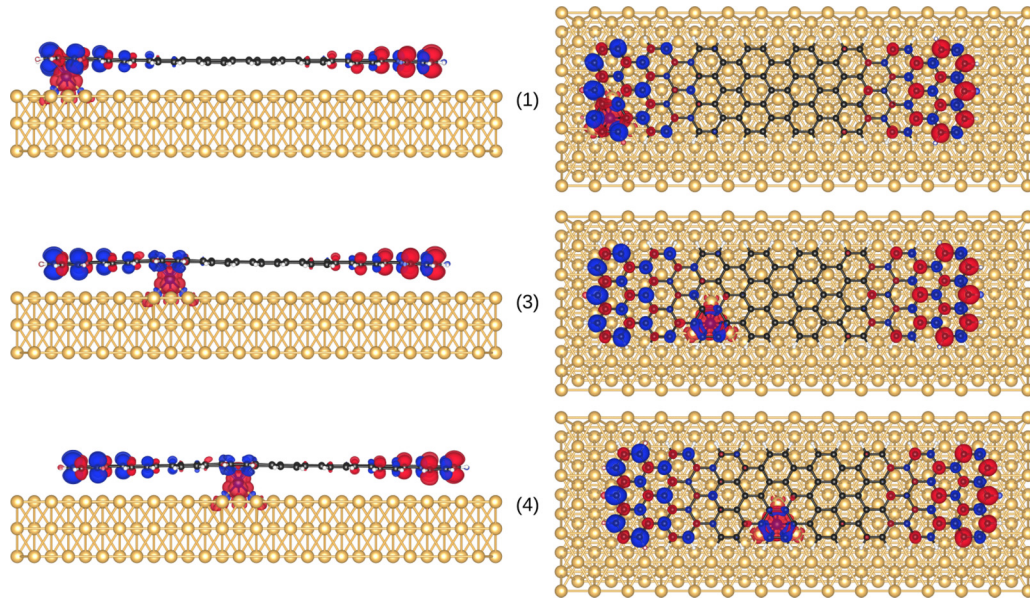


FIG. 5. Calculated magnetization density. Evolution of the magnetization density with the Co atom moving from end state into the GNR's bulk; positions from top to bottom (1,3,4). Red volumes denote spin-up and blue colors spin-down magnetization. (Parameters: isosurface value of  $\pm 0.001 \mu_B/\text{\AA}^3$ ; spin DFT with the PBE exchange-correlation functional [63].)

at the corner, where the Co atom is intercalated (labeled 1),  $dI/dV$  exhibits a peak (black curve) right at  $E_F$ , which is considerably narrower (FWHM of  $28 \pm 14$  mV), resembling a Kondo resonance [31,56–59]. It is predominantly the shift of the peak from above the Fermi level for pristine GNR to right at the Fermi level for Co(1)-GNR that suggests the interpretation as a Kondo signature for Co(1)-GNR. The other possibility, that the end state is merely modified and shifted down in energy to the Fermi level, seems unlikely since it would require a considerable charge transfer of approximately one elementary charge into the highly localized end state.

If interpreted as a Kondo signature, the peak would correspond to a Kondo temperature of  $T_K = 259 \pm 9$  K extracted from a fit (red curve) of an asymmetric Frota line shape [60,61].<sup>2</sup> We note that the system is expected to be unstable against diffusion at elevated temperatures, preventing to assign the zero-bias peak to the Kondo effect from its temperature dependence. Interestingly, the corner adjacent to the intercalated Co atom (labeled 1') shows an essentially featureless spectrum, i.e., the end state vanishes at this corner.

The constant-height current map that is shown in Fig. 4(d) was recorded simultaneously with the AFM image and reflects the spatially resolved local density of states at  $E_F$ . Consistent with the  $dI/dV$  spectra, it reveals a very pronounced LDOS at the site of the intercalated Co atom spreading out a few lattice sites, but no increased LDOS at the adjacent corner at

site 1'. While it is not clear, why the end state is suppressed at the adjacent corner at site 1', we speculate that the former end state hybridizes with atomic Co states and therefore shifts towards the Co atom and away from site 1'.

In total, seven individual Co(1)-GNR complexes of this type were assembled, all showing qualitatively the same spectroscopic fingerprints. The average maximum position was at  $0 \pm 4$  mV exhibiting a mean FWHM of  $30 \pm 10$  mV (the uncertainty margins refer to the standard deviations from the mean value).

*Theory.* The DFT calculations have no direct access to Kondo physics. Apart from artifacts of approximate exchange-correlation functionals, there are also fundamental reasons for this [62]. Nevertheless, studies in approximate spin DFT are useful because they reveal a trend towards magnetism that in more complete theories often translates into the Kondo effect.

*Magnetism.* In this spirit, we show in Fig. 5 the magnetization density resulting from spin DFT. The carbon-based end states exhibit the magnetic moments already expected from the tight-binding analysis. For the Co atom at the corner site 1, the corresponding end state couples antiferromagnetically to the intercalating Co atom (Fig. 5, top row). The corresponding magnetic moment of the Co atom is found to be  $1.7 \mu_B$ – $1.8 \mu_B$ , in good agreement with Ref. [64], representing the spin contribution to the magnetic moment. Thus, we expect two unpaired electrons in the  $3d$  shell and an excess charge of one extra electron, consistent with atomic DOS analysis in the Supplemental Material [43]. The magnetic structure of the  $d$  shell of  $\text{Co}^-$  is broadly understood from conventional arguments of ligand-field theory. With a local neighborhood of the carbon ring above and the three bonding partners from the Au(111)-hollow position below, the environment of  $\text{Co}^-$  implies a predominant  $C_3$  symmetry (weakly broken at the edge) with irreducible representations of  $A-z^2$  and  $E-\{x^2 - y^2,$

<sup>2</sup>Different definitions of the Kondo temperature exist. For the comparability to the Kondo temperatures extracted from previous STM experiments we use the definition  $k_B T_K = 2.54\Gamma$ , where  $k_B$  is the Boltzmann constant and the width  $\Gamma$  of the Frota line is defined in Ref. [61]. We note that an overestimation of  $T_K$  is certainly possible because we are most likely dealing with the half-width of a temperature-broadened logarithmic singularity [76,77].

$xy$ },  $E$ - $\{yz, xz\}$ . The latter two orbitals generate the open shell that supports the majority spin [43]. Although the breaking of the threefold rotational symmetry at the edge and corner is weak in our case, in other systems this reduction of symmetry can have further consequences for the Kondo effect [65,66].

The Co-based Kondo physics usually emanates from strong fluctuations of the magnetic moment residing in the open  $3d$  shell. Since here the moment couples to the end state, one might suspect that spin fluctuations are diminished, with a tendency for the Kondo effect to be quenched. However, our calculations do not support a complete quench. We find that the Co-based moment is approximately the same for all intercalation positions (1,3,4) shown in Fig. 5, and take this as an indication that the magnetic structure of the Co atom is largely resulting from its coupling to the Au substrate. We thus assign the zero-bias anomaly (ZBA) observed in Fig. 4(b) (black trace) to a hybrid state featuring Kondo-like fluctuations that are disturbed due to a subdominant coupling to the end state. The end-state based ZBA is thus qualitatively similar to the ZBA observed for Co also in the absence of end states.

**LDOS.** In Fig. 6 we display the LDOS of the cobalt atom as well as the one of the end states near and far the Co impurity for different complexes depicted in Fig. 5. For all sites considered, the cobalt  $3d$  states are smeared out over an energy range of several electron volts due to the coupling to the gold substrate [43]. The hybridization with a quasicon- tinuum of states is a prerequisite for the Kondo effect and is also present for the Co/Au(111) system without GNR [31]. A direct comparison with a bare adatom is made to scrutinize the influence of the ribbon on the hybridization of cobalt with the substrate. While the broadening of the Co  $3d$  states is dominated by the coupling to the substrate, the interaction with the ribbon gives rise to an appreciable redistribution of the  $3d$ -related spectral weight of the LDOS [43].

We note that the effects related to Kondo physics involve unpaired electron spins and, thus, are sensitive to the LDOS around  $E_F$  within the range of Coulomb charging energy  $U$ . In this respect, for intercalation at the corner site 1, where the influence of ribbon end state is likely to be the strongest, the Co  $3d$  states indeed change considerably close to the Fermi level, as seen in Fig. 6 (top). In particular, at  $\approx 0.3$  eV below  $E_F$  a peak emerges that is absent otherwise. Moreover, this peak coincides with the left end state as can be seen in the DOS for positions 1 and  $1'$  and their overall shape resemble each other. The DOS for carbon ring (1) is reduced with respect to  $1'$  and  $n'$ , signaling a shift of electronic density towards the cobalt atom. All these features hint for orbital hybridization between cobalt and the left ribbon end state. The shift of the DOS peaks (1) and ( $1'$ ) towards lower energies by about 0.15 eV compared to the DOS peak ( $n'$ ) reinforces this interpretation. The increased presence of cobalt states at the Fermi level distinguishes this case from the other intercalation cases (see below).

#### D. Moving from edge to bulk

*Theory.* Combining the analysis of end-state magnetism with the insights from the tight-binding electronic structure, we formulate an expectation (independent of DFT results) about the evolution of the ZBA upon shifting the Co atom

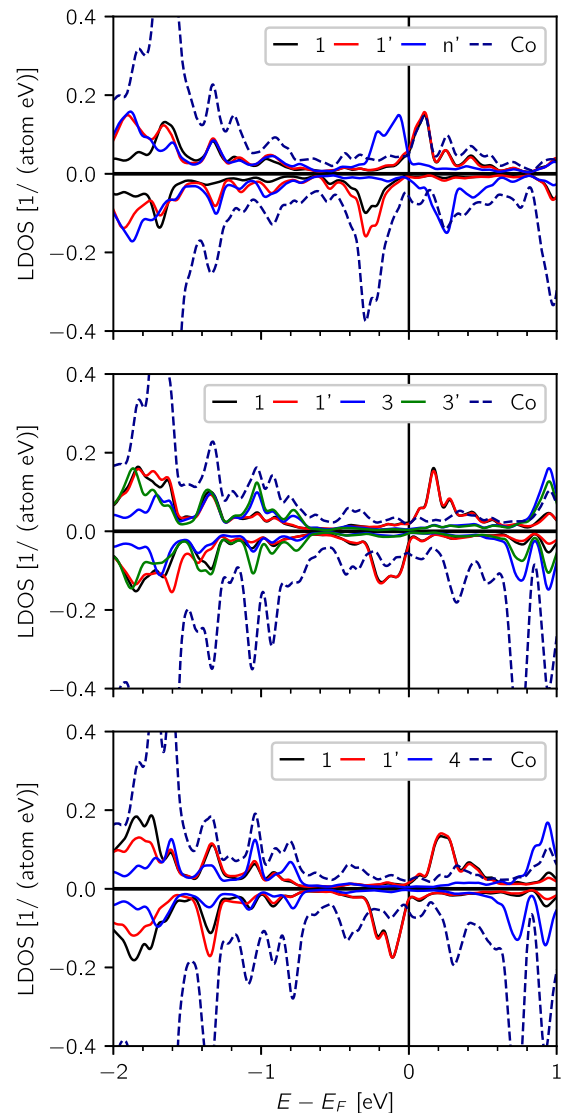


FIG. 6. Calculated LDOS. Electronic structure of cobalt intercalated at sites 1, 3, and 4 from top to bottom. Local density of states with Gaussian smearing of 40 meV. Negative values represent minority-spin states, positive values majority-spin states. Labels correspond to the carbon-ring sites as defined above.

gradually from the corner, site 1, into the bulk, site 4. Along this path the driving agent reshaping the ZBA is the depletion of the LDOS near the Fermi energy. By moving the Co atom away from the end, its coupling to the end-based spin is decreased and the consequence is a resurgence of the full  $3d$ -spin fluctuations and the associated Kondo resonance. Therefore, one expects a certain evolution of the ZBA from an end-state modified hybrid form towards the traditional Kondo shape.

The expectations here formulated are fully consistent with results from a spin-DFT investigation. As expected, the LDOS on the carbon sites in the bulk, positions (3,3',4), is depleted near the Fermi energy exhibiting the bulk gap of about 1.5 eV (Fig. 6 center and bottom). Consequently, at these sites the Co-based LDOS around the Fermi energy is less affected by the ribbon and the hybridization of  $3d$  states

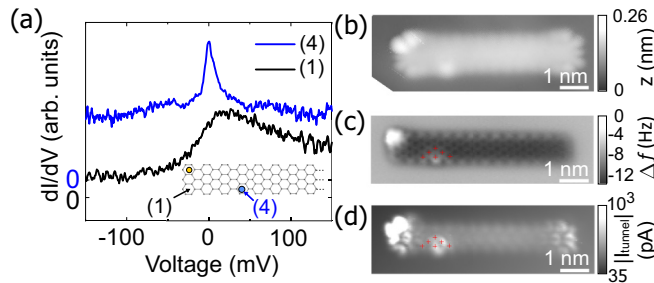


FIG. 7. Co at site 4. (a)  $dI/dV$  spectra of a Co(4)-GNR complex. The inset sketches the intercalation sites of Au and Co atom and indicates the positions the spectra were taken at. (b) STM image ( $V = 4$  mV,  $I = 50$  pA), (c) AFM image, and (d) current map of the complex. Red crosses in (c) and (d) mark the same positions.

mainly reflects the coupling of Co to the Au substrate [43], which also enables the Kondo effect for the case without ribbon [31]. The effect of the end state on the Co atom is only present for intercalation at the corner site and manifests strongest as a resonance enhancement at  $\simeq 0.3$  eV below  $E_F$ , as discussed above. This peak is absent for intercalation at sites 3 and 4. Instead, for intercalation at these sites the Co LDOS displays a peak at  $\simeq 0.7$  eV above  $E_F$  that is absent for intercalation at site 1 (see Fig. 6). This demonstrates that the ribbon-induced redistribution of the  $3d$ -related spectral weight of the LDOS [43] is indeed specific to the intercalation site.

*Experiment.* To scrutinize the Co-GNR interaction and the role of the end state further, we placed adatoms at the GNR armchair edges. Intercalating Co atoms at various positions along the armchair edge, it turned out that up to site 4 [see inset in Fig. 7(a) for labeling] the spectra change significantly with respect to each other, but from there onwards no further modifications are appreciable. We note that position 4 corresponds to a distance of 1.4 nm from the zigzag edge, matching the decay length of the end state reported in Ref. [35]. Hence, as an example for Co at the armchair edge, the data of a Co(4)-GNR complex are presented in Fig. 7. The Co atom intercalated at site 4 at the lower armchair edge appears as bright, round protrusion in the STM topography. Here, in addition to the Co atom, a Au atom was intercalated at site 1', the effect of which will be discussed further below. The AFM image shown in Fig. 7(c) along with the corresponding STM image [Fig. 7(b)] clearly confirms the intercalation geometry. The more repulsive features of the graphene lattice around the intercalation positions reflect lifting of the ribbon slightly away from the surface.

The  $dI/dV$  spectrum acquired at the position of the intercalated Co atom exhibits a pronounced zero-bias peak [Fig. 7(a), blue curve] at  $0 \pm 3$  mV having a FWHM of  $9 \pm 7$  mV. This is even narrower than the peak observed at Co atoms intercalated at the corner of aGNR. For comparison, a spectrum acquired at the nonintercalated corner is shown as black curve. We further note that a GNR-armchair edge exhibits spectra that are basically featureless around  $E_F$ .

The appearance of a zero-bias peak upon intercalation of Co therefore suggests its interpretation as a Kondo resonance with  $T_K = 88 \pm 5$  K. The observation of Kondo signatures

for similar systems [64,67] further supports this interpretation. The Au atom intercalated at site 1' seems not to have a significant effect on site 4 where the influence of the end state effectively dies out. It is independently verified with a clean Co(4)-GNR complex (no Au atom intercalated). We, indeed, observed a very similar spectral feature at  $E_F$ , exhibiting a Kondo temperature comparable to that of the Co(4)-Au(1')-GNR [43].

As the armchair edge of GNRs does not host electronic states around  $E_F$ , the Kondo effect is assumed to be due to the interaction of the Co atom with the Au(111) substrate. The shape of the Kondo feature in this Co-GNR complex, however, is distinctly different from the one of an isolated Co atom on the Au(111) surface [68]. The latter exhibits a dip in differential conductance at zero bias as opposed to the peak observed for the Co-GNR complex. The different appearance of a Kondo feature as a peak or dip shape is a consequence of the quantum interference between different tunneling pathways [31,68] and their different magnitudes, where the presence of the GNR apparently changes the ratio of different tunneling pathways in favor of direct tunneling into the impurity state. A current map acquired at constant height and a bias voltage of  $|V| \sim 1$  mV is shown in Fig. 7(d) and provides insight into the spatial distribution of the Kondo feature. The current at low bias is enhanced at Co-intercalation position and at the GNR zigzag ends, while the left GNR zigzag edge appears particularly intense because of the intercalated Au atom at position 1'. The enhanced current close to the position of Co intercalation, reflecting the spatial distribution of the corresponding zero-bias feature, is quite localized around the intercalation position, extends slightly towards the GNR center, but appears well separated from the features at the GNR ends. This is consistent with the aforementioned assumption that a Co atom intercalated at site 4 is sufficiently far away from the zigzag edge to avoid coupling to the latter. Interestingly, the feature around the intercalation position exhibits a pronounced nodal plane structure. Note that, when interpreting the nodal plane structure, the enhanced  $p$ -wave tunneling of the CO-functionalized tip has to be taken into consideration [69].

In total, eight different Co-GNR complexes with a Co atom buried at the middle of the armchair edge were created and characterized, yielding consistent results with a relatively narrow, Kondo-type resonance at  $3 \pm 3$  mV and a FWHM of  $20 \pm 8$  mV. The uncertainty margins refer to the standard deviation.

*Co between end and bulk.* As an intermediate case between intercalation at the corner position and at the armchair edge, a Co atom was manipulated underneath the third hexagon counted from the zigzag end, creating a Co(3)-GNR complex (see Fig. 8). The STM image shown in Fig. 8(a) exhibits the characteristic fingerlike structure of the end state and a slight protrusion at the intercalation position. Due to their close vicinity, these two features blend into each other.

The corresponding AFM image [Fig. 8(c)] confirms the intercalation position and exhibits a similar increase in repulsion of the GNR, interpreted as a local upward bending of the GNR as discussed above. (The fourfold feature in the image below the GNR presumably relates to a hydrogen atom that got trapped there.)

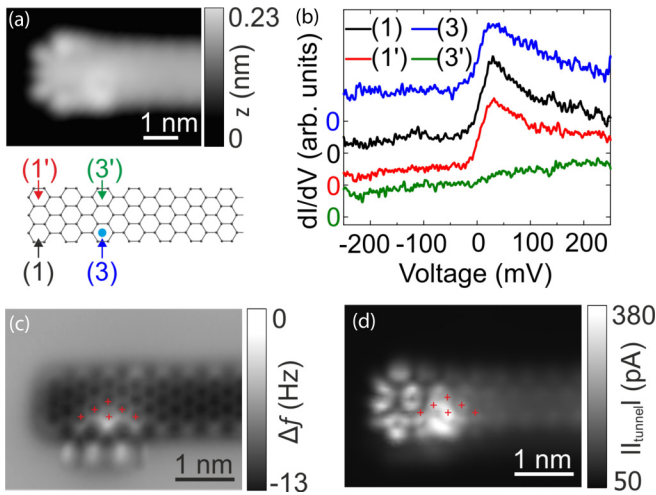


FIG. 8. Co at site 3. (a) Upper panel: STM image ( $V = 5$  mV,  $I = 30$  pA, mild Gaussian smoothing applied). Lower panel: sketch of Co intercalation position. (b)  $dI/dV$  spectra taken at positions indicated in (a). (c) Constant height AFM image of the Co(3)-GNR complex shown in (a). The protrusions below the GNR are presumably artifacts from a H atom, trapped below the tip and dragged along while scanning. (d) Current map of the area shown in (c). The red crosses in (c) and (d) mark the same positions.

Figure 8(b) shows  $dI/dV$  spectra acquired at different positions. The two spectra acquired at the corners 1 and 1' as well as the one acquired at the intercalation position are very similar and exhibit the typical shape as observed for clean zigzag edges, namely, a peak considerably away from zero bias at  $30 \pm 3$  mV, with a strongly asymmetric shape and a FWHM of  $52 \pm 35$  mV. Conversely, a spectrum acquired at position 3', that is, at the clean armchair edge at the same distance from the zigzag edge as the intercalated Co atom, is featureless.

Hence, the Co(3)-GNR configuration does not exhibit a Kondo-type resonance. Instead, the zigzag end state seems to be extended to the Co intercalation position. The latter observation is supported by the current map presented in Fig. 8(d), showing that also for low bias the features around the Co atom position and the GNR end blend into each other. Also, a pronounced nodal-plane structure is evident in the current image.

Co(3)-GNR complexes were assembled three times, all showing an apparent extension of the end state up to the position of the intercalated Co atom and no zero-bias peak.

*Discussion.* A comparison of DFT calculations with experimental findings starts with the observation that the key qualitative expectation is being met: While a sharp Kondo resonance is measured near the Co atom at a bulk position (Fig. 7), a significantly broader zero-bias anomaly is found for a Co atom at the edge (Fig. 4), indicating the strong interaction between the Kondo resonance and the edge state. Beyond this, many interesting details are discovered in the experiment, which escape a straightforward DFT-based interpretation. The most striking example is the drastic change of the spectra when moving the Co atom between the two neighboring positions 4 and 3 (see Figs. 7 and 8). Based on the experimental observations one might assume that the



FIG. 9. Au and Co at one GNR. STM image of a GNR with an intercalated Co (bottom left corner) and Au (top right corner) atom. 2 mV,  $I = 48$  pA.

Co spin in position 3 is quenched, but the DFT calculation in Fig. 5 yields a nonvanishing spin in this geometry. So, either there is a physical effect at play that lies outside of the standard exchange-correlation description of DFT or the assumptions concerning the atomic structure underlying the DFT simulation do not fully reflect experimental conditions.

To rationalize the experimental finding in the passage towards bulk from the ribbon corner, one might speculate on the following scenario. At sites far away from the corner, the electronic states associated to Co atom close to the Fermi energy hybridize mainly with that of the gold substrate, and not (or very weakly) with the GNR as it exhibits an energy gap, making the situation similar to an isolated Co on Au(111). However, closer to the corner, the Co-based Kondo ZBA starts to interfere with the GNR end state. In this situation, one certainly expects a ZBA to survive, but any details are difficult to predict, partly because the result will depend on the mutual interference of dominant tunneling paths. When moved to the corner, the orbitals start to hybridize with the GNR end state and the weak-coupling picture no longer applies, with a general expectation that the Kondo physics survives.

### E. Au atom at corner position for comparison

To investigate the role of the species of the intercalated atom, for comparison, a Au atom was intercalated at the corner of a GNR. Single Au atoms were brought onto the Au(111) surface by gentle tip indentations into the Au surface. As opposed to Co adatoms, isolated Au adatoms on the Au(111) surface show no Kondo features. The Au-GNR complexes were created in the same way as the Co-GNR complexes by atomic manipulation.

Figure 9 shows an STM image of a GNR with a Co atom intercalated at one corner and a Au atom at the corner of the opposite end of the same GNR. As we assume that they do not interact, both sites can be labeled as site 1. The two corners appear qualitatively different. Whereas the Co corner appears more roundish, the Au corner retains the fingerlike structure typical of the end state. The Au-intercalated corner appears considerably brighter in the STM image, possibly because of a stronger upward bending of the GNR upon intercalation. Figure 10(a) shows an STM image of a Au(1)-GNR complex (left) next to a pristine GNR end (right). The colored circles indicate the locations of the  $dI/dV$  spectra displayed in Fig. 10(b). The spectrum taken at a corner of the pristine GNR (red curve) exhibits the typical end-state peak. The peak maximum lies at  $6 \pm 3$  mV and the FWHM of  $16 \pm 8$  mV is relatively narrow in this case.

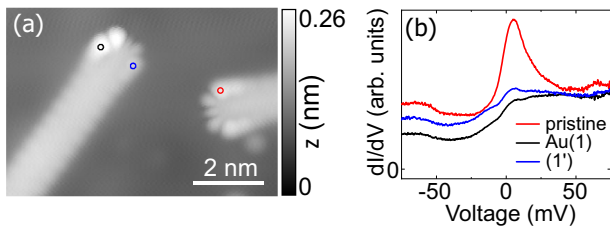


FIG. 10. Au at corner position. (a) STM image of a Au(1)-GNR complex (left) next to a pristine GNR end (right).  $V = 2$  mV,  $I = 48$  pA. (b)  $dI/dV$  spectra taken at the positions indicated by colored circles in (a).

At the Au-intercalated corner (black line), however, a clear peak is missing in the spectrum. The same holds true for the corner  $1'$  next to the intercalated Au atom (blue curve). Instead, one can see a slight increase in  $dI/dV$  from negative voltages of  $-30$  mV towards 0 (like an onset), after which the signal remains roughly constant.

The spatial fingerlike feature seen in the images, however, clearly indicates that the GNR end state is still present and also localized at the Au-intercalation position. Taking together both observations suggests that the presence of the Au atom smears out the end state in energy, such that it is barely visible in  $dI/dV$  spectra, while its presence is evident from its spatial signature.

The strong geometric upward bending of the GNR zigzag end by the Au atom is seen in the AFM image in Fig. 7(c), in which besides the Co atom at the armchair edge a Au atom was intercalated at one of the corner sites.

The Au intercalation shows that the presence of an intercalated atom alone is not enough to convert the end state into a zero-bias resonance. Instead, the appearance of the latter is apparently related to the magnetic properties of the Co adatoms.

### III. SUMMARY AND CONCLUSION

7-aGNRs were synthesized under UHV conditions on a Au(111) surface. Subsequently added Co atoms were intercalated by means of atomic manipulation underneath different sites in a well-controlled fashion. Whereas Co atoms on Au(111) show a Kondo dip in differential conductance spectra, the Co-GNR complexes exhibit a peak. Our main finding is that the shape of the peak depends on the intercalation position along the GNR armchair edge: a Co atom intercalated at the GNR corner yields a zero-bias resonance, with its maximum at  $0 \pm 4$  mV and a FWHM of  $30 \pm 10$  mV. Co atoms buried at the armchair edge away from the GNR corner display an even narrower zero-bias resonance centered at  $3 \pm 3$  mV having a FWHM of  $20 \pm 8$  mV, well separated from the GNR end state. Surprisingly, a Co atom placed at an intermediate distance from the corner leads to the end-state peak extending towards the Co atom, with no signs of a zero-bias resonance.

The key experimental result, i.e., the narrowing of the Kondo resonance when moving the Co atom from edge to bulk, has been corroborated by extensive density functional theory (DFT) calculations. In particular, DFT gives strong and

transparent indication of the presence of magnetic moments. It does not hint at why the Kondo signal gets lost intermittently along the passage of the Co atom from edge to bulk, as is seen in the measurement.

In conclusion, our study clearly demonstrates the potential that graphene nanoribbons exhibit as a laboratory to study the interplay of the Kondo effect with other zero-bias anomalies. Regimes of strong coupling and weak coupling can be addressed with an intermediate range that exhibits intriguing phenomena that remain to be understood.

### IV. METHODS

*Experiment.* Experiments were performed with a custom-built combined scanning tunneling and frequency-modulation atomic force microscope (STM/AFM) operating in ultrahigh vacuum (base pressure  $p < 5 \times 10^{-11}$  mbar) and at a base temperature of about 9 K. The combined STM/AFM system is equipped with a qPlus [70] sensor that allows one to measure the tunneling current  $I$  and frequency shift ( $\Delta f$ ) simultaneously. Bias voltages  $V$  refer to the sample bias with respect to the tip. Au(111) single-crystal surface was cleaned by repeated  $\text{Ne}^+$  sputtering and annealing cycles. 7-aGNRs were grown from 10,10'-dibromo-9,9'-bianthracene precursors following the recipe introduced by Cai *et al.* [9]. Co atoms were deposited onto the cold sample surface located inside the STM/AFM. AFM images were taken with a CO-functionalized tip [71]. To this end, in the corresponding experiments, NaCl in very small amounts was codeposited after the synthesis of the 7-aGNRs at room temperature, while CO molecules were coadsorbed onto the cold sample surface located inside the STM/AFM. This enabled a controlled CO termination of the scanning probe tip with picking up of an individual CO molecule from NaCl island. For STM images and spectroscopy, metallic tip apexes were used, unless stated explicitly otherwise.

*Ab initio calculation.* We perform density functional theory (DFT) calculations using QUANTUM ESPRESSO[72]. Graphene ribbons on a gold surface are modeled by placing a 7-aGNR (comprising 8 anthracene units), saturated with hydrogen atoms, on top of a three-layer Au(111) slab. This is a computational compromise as we already deal with a relatively large system with 403 atoms. Cobalt atoms are intercalated such that the position of the sites, the center of the hexagonal carbon rings, coincides with an hcp position of the Au(111) surface.

We employ norm-conserving pseudopotentials for carbon, hydrogen, cobalt, and gold atoms. We use the Perdew-Burke-Ernzerhoff (PBE) exchange-correlation potential [63]. In our calculations a plane-wave energy cutoff of 70 Ry and a 280-Ry cutoff for the density and potential representation are chosen to ensure converged calculations. We account for the dispersion of the gold surface by a Brillouin zone sampling of  $2 \times 2$ , effectively corresponding to a sampling of  $20 \times 8$  for the fcc geometry. A vacuum of 10 Å is introduced between the gold layers to reduce interactions among the slabs, which is a tradeoff between accuracy and reduced computational complexity. We correct for van der Waals interactions by adding semiempirical interaction potentials for the different atom pairs [73].



Onsite Coulomb interactions in the cobalt  $3d$  orbitals are known to be poorly described by standard DFT, which is why we apply a Hubbard  $U$  of 5 eV [74]. We determined the Hubbard  $U$  by occupation interpolation via linear response theory [74] at different sites, a value which is in accordance with similar studies [64].

## ACKNOWLEDGMENTS

Funding from the Deutsche Forschungsgemeinschaft (DFG, German Research Foundation) through CRC 689 and 314695032 (CRC 1277) subprojects A09, B01, and B07 is gratefully acknowledged.

S.K., T.F., and T.P. contributed equally to this work.

- 
- [1] Y.-W. Son, M. L. Cohen, and S. G. Louie, Energy Gaps in Graphene Nanoribbons, *Phys. Rev. Lett.* **97**, 216803 (2006).
- [2] V. Barone, O. Hod, and G. E. Scuseria, Electronic structure and stability of semiconducting graphene nanoribbons, *Nano Lett.* **6**, 2748 (2006).
- [3] M. Y. Han, B. Özyilmaz, Y. Zhang, and P. Kim, Energy Band-Gap Engineering of Graphene Nanoribbons, *Phys. Rev. Lett.* **98**, 206805 (2007).
- [4] H. Zhang, H. Lin, K. Sun, L. Chen, Y. Zagranyarski, N. Aghdassi, S. Duhm, Q. Li, D. Zhong, Y. Li, K. Müllen, H. Fuchs, and L. Chi, On-surface synthesis of rylene-type graphene nanoribbons, *J. Am. Chem. Soc.* **137**, 4022 (2015).
- [5] N. Merino-Díez, A. García-Lekue, E. Carbonell-Sanromà, J. Li, M. Corso, L. Colazzo, F. Sedona, D. Sánchez-Portal, J. I. Pascual, and D. G. de Oteyza, Width-dependent band gap in armchair graphene nanoribbons reveals fermi level pinning on  $au(111)$ , *ACS Nano* **11**, 11661 (2017).
- [6] L. Talirz, H. Söde, T. Dumlaff, S. Wang, J. R. Sanchez-Valencia, J. Liu, P. Shinde, C. A. Pignedoli, L. Liang, V. Meunier, N. C. Plumb, M. Shi, X. Feng, A. Narita, K. Müllen, R. Fasel, and P. Ruffieux, On-surface synthesis and characterization of 9-atom wide armchair graphene nanoribbons, *ACS Nano* **11**, 1380 (2017).
- [7] Y.-C. Chen, D. G. de Oteyza, Z. Pedramrazi, C. Chen, F. R. Fischer, and M. F. Crommie, Tuning the band gap of graphene nanoribbons synthesized from molecular precursors, *ACS Nano* **7**, 6123 (2013).
- [8] H. Huang, D. Wei, J. Sun, S. L. Wong, Y. P. Feng, A. H. C. Neto, and A. T. S. Wee, Spatially resolved electronic structures of atomically precise armchair graphene nanoribbons, *Sci. Rep.* **2**, 983 (2012).
- [9] J. Cai, P. Ruffieux, R. Jaafar, M. Bieri, T. Braun, S. Blankenburg, M. Muoth, A. P. Seitsonen, M. Saleh, X. Feng, K. Müllen, and R. Fasel, Atomically precise bottom-up fabrication of graphene nanoribbons, *Nature (London)* **466**, 470 (2010).
- [10] P. Ruffieux, S. Wang, B. Yang, C. Sánchez-Sánchez, J. Liu, T. Dienel, L. Talirz, P. Shinde, C. A. Pignedoli, D. Passerone, T. Dumlaff, X. Feng, K. Müllen, and R. Fasel, On-surface synthesis of graphene nanoribbons with zigzag edge topology, *Nature (London)* **531**, 489 (2016).
- [11] D. G. de Oteyza, A. García-Lekue, M. Vilas-Varela, N. Merino-Díez, E. Carbonell-Sanromà, M. Corso, G. Vasseur, C. Rogero, E. Guitián, J. I. Pascual, J. E. Ortega, Y. Wakayama, and D. Peña, Substrate-independent growth of atomically precise chiral graphene nanoribbons, *ACS Nano* **10**, 9000 (2016).
- [12] J. Liu, B.-W. Li, Y.-Z. Tan, A. Giannakopoulos, C. Sanchez-Sanchez, D. Beljonne, P. Ruffieux, R. Fasel, X. Feng, and K. Müllen, Toward cove-edged low band gap graphene nanoribbons, *J. Am. Chem. Soc.* **137**, 6097 (2015).
- [13] R. Pawlak, X. Liu, S. Ninova, P. D'Astolfo, C. Drechsel, S. Sangtarash, R. Häner, S. Decurtins, H. Sadeghi, C. J. Lambert, U. Aschauer, S.-X. Liu, and E. Meyer, Bottom-up synthesis of nitrogen-doped porous graphene nanoribbons, *J. Am. Chem. Soc.* **142**, 12568 (2020).
- [14] S. Kawai, S. Saito, S. Osumi, S. Yamaguchi, A. S. Foster, P. Spijker, and E. Meyer, Atomically controlled substitutional boron-doping of graphene nanoribbons, *Nat. Commun.* **6**, 8098 (2015).
- [15] R. R. Cloke, T. Marangoni, G. D. Nguyen, T. Joshi, D. J. Rizzo, C. Bronner, T. Cao, S. G. Louie, M. F. Crommie, and F. R. Fischer, Site-specific substitutional boron doping of semiconducting armchair graphene nanoribbons, *J. Am. Chem. Soc.* **137**, 8872 (2015).
- [16] C. Bronner, S. Strelau, M. Gille, F. Brauße, A. Haase, S. Hecht, and P. Tegeder, Aligning the band gap of graphene nanoribbons by monomer doping, *Angew. Chem. Int. Ed.* **52**, 4422 (2013).
- [17] S. Kawai, S. Nakatsuka, T. Hatakeyama, R. Pawlak, T. Meier, J. Tracey, E. Meyer, and A. S. Foster, Multiple heteroatom substitution to graphene nanoribbon, *Sci. Adv.* **4**, eaar7181 (2018).
- [18] T. Cao, F. Zhao, and S. G. Louie, Topological Phases in Graphene Nanoribbons: Junction States, Spin Centers, and Quantum Spin Chains, *Phys. Rev. Lett.* **119**, 076401 (2017).
- [19] O. Gröning, S. Wang, X. Yao, C. A. Pignedoli, G. Borin Barin, C. Daniels, A. Cupo, V. Meunier, X. Feng, A. Narita, K. Müllen, P. Ruffieux, and R. Fasel, Engineering of robust topological quantum phases in graphene nanoribbons, *Nature (London)* **560**, 209 (2018).
- [20] D. J. Rizzo, G. Veber, T. Cao, C. Bronner, T. Chen, F. Zhao, H. Rodriguez, S. G. Louie, M. F. Crommie, and F. R. Fischer, Topological band engineering of graphene nanoribbons, *Nature (London)* **560**, 204 (2018).
- [21] S. Okada, M. Igami, K. Nakada, and A. Oshiyama, Border states in heterosheets with hexagonal symmetry, *Phys. Rev. B* **62**, 9896 (2000).
- [22] M. Fujita, K. Wakabayashi, K. Nakada, and K. Kusakabe, Peculiar localized state at zigzag graphite edge, *J. Phys. Soc. Jpn.* **65**, 1920 (1996).
- [23] K. Nakada, M. Fujita, G. Dresselhaus, and M. S. Dresselhaus, Edge state in graphene ribbons: Nanometer size effect and edge shape dependence, *Phys. Rev. B* **54**, 17954 (1996).
- [24] Y. Miyamoto, K. Nakada, and M. Fujita, First-principles study of edge states of H-terminated graphitic ribbons, *Phys. Rev. B* **59**, 9858 (1999).
- [25] N. Friedrich, P. Brandimarte, J. Li, S. Saito, S. Yamaguchi, I. Pozo, D. Peña, T. Frederiksen, A. Garcia-Lekue, D. Sánchez-Portal, and J. I. Pascual, Magnetism of Topological Boundary States Induced by Boron Substitution in Graphene Nanoribbons, *Phys. Rev. Lett.* **125**, 146801 (2020).

- [26] J. Li, S. Sanz, J. Castro-Esteban, M. Vilas-Varela, N. Friedrich, T. Frederiksen, D. Peña, and J. I. Pascual, Uncovering the Triplet Ground State of Triangular Graphene Nanoflakes Engineered with Atomic Precision on a Metal Surface, *Phys. Rev. Lett.* **124**, 177201 (2020).
- [27] A. K. Mitchell, D. Schuricht, M. Vojta, and L. Fritz, Kondo effect on the surface of three-dimensional topological insulators: Signatures in scanning tunneling spectroscopy, *Phys. Rev. B* **87**, 075430 (2013).
- [28] L. Fritz and M. Vojta, Phase transitions in the pseudogap anderson and kondo models: Critical dimensions, renormalization group, and local-moment criticality, *Phys. Rev. B* **70**, 214427 (2004).
- [29] Y. Li, A. T. Ngo, A. DiLullo, K. Z. Latt, H. Kersell, B. Fisher, P. Zapol, S. E. Ulloa, and S.-W. Hla, Anomalous Kondo resonance mediated by semiconducting graphene nanoribbons in a molecular heterostructure, *Nat. Commun.* **8**, 946 (2017).
- [30] X. Su, Z. Xue, G. Li, and P. Yu, Edge state engineering of graphene nanoribbons, *Nano Lett.* **18**, 5744 (2018).
- [31] M. Ternes, A. J. Heinrich, and W.-D. Schneider, Spectroscopic manifestations of the Kondo effect on single adatoms, *J. Phys.: Condens. Matter* **21**, 053001 (2009).
- [32] F. Evers, R. Korytár, S. Tewari, and J. M. van Ruitenbeek, Advances and challenges in single-molecule electron transport, *Rev. Mod. Phys.* **92**, 035001 (2020).
- [33] M. Koch, F. Ample, C. Joachim, and L. Grill, Voltage-dependent conductance of a single graphene nanoribbon, *Nat. Nanotechnol.* **7**, 713 (2012).
- [34] J. van der Lit, M. P. Boneschanscher, D. Vanmaekelbergh, M. Ijäs, A. Uppstu, M. Ervasti, A. Harju, P. Liljeroth, and I. Swart, Suppression of electron-vibron coupling in graphene nanoribbons contacted via a single atom, *Nat. Commun.* **4**, 2023 (2013).
- [35] S. Wang, L. Talirz, C. A. Pignedoli, X. Feng, K. Müllen, R. Fasel, and P. Ruffieux, Giant edge state splitting at atomically precise graphene zigzag edges, *Nat. Commun.* **7**, 11507 (2016).
- [36] M. Ijäs, M. Ervasti, A. Uppstu, P. Liljeroth, J. van der Lit, I. Swart, and A. Harju, Electronic states in finite graphene nanoribbons: Effect of charging and defects, *Phys. Rev. B* **88**, 075429 (2013).
- [37] L. Talirz, H. Söde, J. Cai, P. Ruffieux, S. Blankenburg, R. Jafaar, R. Berger, X. Feng, K. Müllen, D. Passerone, R. Fasel, and C. A. Pignedoli, Termini of bottom-up fabricated graphene nanoribbons, *J. Am. Chem. Soc.* **135**, 2060 (2013).
- [38] H. Lee, Y.-W. Son, N. Park, S. Han, and J. Yu, Magnetic ordering at the edges of graphitic fragments: magnetic tail interactions between the edge-localized states, *Phys. Rev. B* **72**, 174431 (2005).
- [39] L. Pisani, J. A. Chan, B. Montanari, and N. M. Harrison, Electronic structure and magnetic properties of graphitic ribbons, *Phys. Rev. B* **75**, 064418 (2007).
- [40] E. H. Lieb, Two theorems on the Hubbard model, *Phys. Rev. Lett.* **62**, 1201 (1989).
- [41] D. M. Eigler and E. K. Schweizer, Positioning single atoms with a scanning tunnelling microscope, *Nature (London)* **344**, 524 (1990).
- [42] J. A. Stroscio and D. M. Eigler, Atomic and molecular manipulation with the scanning tunneling microscope, *Science* **254**, 1319 (1991).
- [43] See Supplemental Material at <http://link.aps.org/supplemental/10.1103/PhysRevB.105.205410> for the calculated intercalation energetics, the hybridization of cobalt states, the cobalt magnetic moment, the appearance of Co on top of ribbons, and spectra of Co(4)-GNR without Au.
- [44] G. Giovannetti, P. A. Khomyakov, G. Brocks, V. M. Karpan, J. van den Brink, and P. J. Kelly, Doping Graphene with Metal Contacts, *Phys. Rev. Lett.* **101**, 026803 (2008).
- [45] S. Mishra, D. Beyer, K. Eimre, S. Kezilebieke, R. Berger, O. Gröning, C. A. Pignedoli, K. Müllen, P. Liljeroth, P. Ruffieux, X. Feng, and R. Fasel, Topological frustration induces unconventional magnetism in a nanographene, *Nat. Nanotechnol.* **15**, 22 (2020).
- [46] A. H. Castro Neto, F. Guinea, N. M. R. Peres, K. S. Novoselov, and A. K. Geim, The electronic properties of graphene, *Rev. Mod. Phys.* **81**, 109 (2009).
- [47] A. Dasgupta, S. Bera, F. Evers, and M. J. van Setten, Quantum size effects in the atomistic structure of armchair nanoribbons, *Phys. Rev. B* **85**, 125433 (2012).
- [48] C. A. Coulson and G. S. Rushbrooke, Note on the method of molecular orbitals, *Math. Proc. Cambridge Philos. Soc.* **36**, 193 (1940).
- [49] S. Mishra, T. G. Lohr, C. A. Pignedoli, J. Liu, R. Berger, J. I. Urgel, K. Müllen, X. Feng, P. Ruffieux, and R. Fasel, Tailoring bond topologies in open-shell graphene nanostructures, *ACS Nano* **12**, 11917 (2018).
- [50] Y.-L. Lee, F. Zhao, T. Cao, J. Ihm, and S. G. Louie, Topological phases in cove-edged and chevron graphene nanoribbons: geometric structures,  $z_2$  invariants, and junction states, *Nano Lett.* **18**, 7247 (2018).
- [51] Z. Chen, A. Narita, and K. Müllen, Graphene nanoribbons: on-surface synthesis and integration into electronic devices, *Adv. Mater.* **32**, 2001893 (2020).
- [52] K. T. Chan, J. B. Neaton, and M. L. Cohen, First-principles study of metal adatom adsorption on graphene, *Phys. Rev. B* **77**, 235430 (2008).
- [53] A. Ishii, M. Yamamoto, H. Asano, and K. Fujiwara, DFT calculation for adatom adsorption on graphene sheet as a prototype of carbon nanotube functionalization, *J. Phys.: Conf. Ser.* **100**, 052087 (2008).
- [54] H. Sevinçli, M. Topsakal, E. Durgun, and S. Ciraci, Electronic and magnetic properties of  $3d$  transition-metal atom adsorbed graphene and graphene nanoribbons, *Phys. Rev. B* **77**, 195434 (2008).
- [55] F. Mohn, L. Gross, and G. Meyer, Measuring the short-range force field above a single molecule with atomic resolution, *Appl. Phys. Lett.* **99**, 053106 (2011).
- [56] U. G. E. Perera, H. J. Kulik, V. Iancu, L. G. G. V. Dias da Silva, S. E. Ulloa, N. Marzari, and S.-W. Hla, Spatially Extended Kondo State in Magnetic Molecules Induced by Interfacial Charge Transfer, *Phys. Rev. Lett.* **105**, 106601 (2010).
- [57] A. Zhao, Q. Li, L. Chen, H. Xiang, W. Wang, S. Pan, B. Wang, X. Xiao, J. Yang, J. G. Hou, and Q. Zhu, Controlling the Kondo effect of an adsorbed magnetic ion through its chemical bonding, *Science* **309**, 1542 (2005).
- [58] S. Karan, D. Jacob, M. Karolak, C. Hamann, Y. Wang, A. Weismann, A. I. Lichtenstein, and R. Berndt, Shifting the Voltage Drop in Electron Transport Through a Single Molecule, *Phys. Rev. Lett.* **115**, 016802 (2015).
- [59] S. Karan, N. Li, Y. Zhang, Y. He, I.-Po Hong, H. Song, J.-T. Lü, Y. Wang, L. Peng, K. Wu, G. S. Michelitsch, R. J. Maurer, K. Diller, K. Reuter, A. Weismann, and R. Berndt, Spin

- Manipulation by Creation of Single-Molecule Radical Cations, *Phys. Rev. Lett.* **116**, 027201 (2016).
- [60] H. O. Frota, Shape of the kondo resonance, *Phys. Rev. B* **45**, 1096 (1992).
- [61] H. Prüser, M. Wenderoth, A. Weismann, and R. G. Ulbrich, Mapping Itinerant Electrons around Kondo Impurities, *Phys. Rev. Lett.* **108**, 166604 (2012).
- [62] M. Thoss and F. Evers, Perspective: Theory of quantum transport in molecular junctions, *J. Chem. Phys.* **148**, 030901 (2018).
- [63] J. P. Perdew, K. Burke, and M. Ernzerhof, Generalized Gradient Approximation Made Simple, *Phys. Rev. Lett.* **77**, 3865 (1996).
- [64] C. Zhou, H. Shan, B. Li, A. Zhao, and B. Wang, Engineering hybrid Co-picene structures with variable spin coupling, *Appl. Phys. Lett.* **108**, 171601 (2016).
- [65] T. Knaak, M. Gruber, C. Lindström, M.-L. Bocquet, J. Heck, and R. Berndt, Ligand-induced energy shift and localization of Kondo resonances in cobalt-based complexes on Cu(111), *Nano Lett.* **17**, 7146 (2017).
- [66] G. E. Pacchioni, M. Pivetta, L. Gragnaniello, F. Donati, G. Autès, O. V. Yazyev, S. Rusponi, and H. Brune, Two-orbital Kondo screening in a self-assembled metal-organic complex, *ACS Nano* **11**, 2675 (2017).
- [67] V. Iancu, K.-F. Braun, K. Schouteden, and C. Van Haesendonck, Inducing Magnetism in Pure Organic Molecules by Single Magnetic Atom Doping, *Phys. Rev. Lett.* **113**, 106102 (2014).
- [68] V. Madhavan, W. Chen, T. Jamneala, M. F. Crommie, and N. S. Wingreen, Local spectroscopy of a Kondo impurity: Co on au(111), *Phys. Rev. B* **64**, 165412 (2001).
- [69] L. Gross, N. Moll, F. Mohn, A. Curioni, G. Meyer, F. Hanke, and M. Persson, High-Resolution Molecular Orbital Imaging Using a *p*-Wave STM Tip, *Phys. Rev. Lett.* **107**, 086101 (2011).
- [70] F. J. Giessibl, Atomic resolution on Si(111)-(7 × 7) by noncontact atomic force microscopy with a force sensor based on a quartz tuning fork, *Appl. Phys. Lett.* **76**, 1470 (2000).
- [71] L. Gross, F. Mohn, N. Moll, P. Liljeroth, and G. Meyer, The chemical structure of a molecule resolved by atomic force microscopy, *Science* **325**, 1110 (2009).
- [72] P. Giannozzi, S. Baroni, N. Bonini, M. Calandra, R. Car, C. Cavazzoni, D. Ceresoli, G. L. Chiarotti, M. Cococcioni, I. Dabo, A. Dal Corso, S. De Gironcoli, S. Fabris, G. Fratesi, R. Gebauer, U. Gerstmann, C. Gougoussis, A. Kokalj, M. Lazzeri, L. Martin-Samos *et al.*, QUANTUM ESPRESSO: A modular and open-source software project for quantum simulations of materials, *J. Phys.: Condens. Matter* **21**, 395502 (2009).
- [73] S. Grimme, Semiempirical GGA-type density functional constructed with a long-range dispersion correction, *J. Comput. Chem.* **27**, 1787 (2006).
- [74] M. Cococcioni and S. de Gironcoli, Linear response approach to the calculation of the effective interaction parameters in the *LDA + U* method, *Phys. Rev. B* **71**, 035105 (2005).
- [75] P. A. Khomyakov, G. Giovannetti, P. C. Rusu, G. Brocks, J. van den Brink, and P. J. Kelly, First-principles study of the interaction and charge transfer between graphene and metals, *Phys. Rev. B* **79**, 195425 (2009).
- [76] Y.-h. Zhang, S. Kahle, T. Herden, C. Stroh, M. Mayor, U. Schlickum, M. Ternes, P. Wahl, and K. Kern, Temperature and magnetic field dependence of a Kondo system in the weak coupling regime, *Nat. Commun.* **4**, 2110 (2013).
- [77] M. Žonda, O. Stetsovych, R. Korytár, M. Ternes, R. Temirov, A. Raccanelli, F. S. Tautz, P. Jelínek, T. Novotný, and M. Švec, Resolving ambiguity of the Kondo temperature determination in mechanically tunable single-molecule Kondo systems, *J. Phys. Chem. Lett.* **12**, 6320 (2021).